Signal Processing with 4 Chip Cascade

Oct, 2018

Contact: Texas Instruments Incorporated
20450 Century Boulevard
Germantown, MD 20874
Web: www.ti.com

Document Revision History

Version	Date	Author(s)	Notes
0.0.1	June, 2018	Dan Wang	Initial draft for MIMO
0.0.2	Oct, 2018	Dan Wang	Add TX beamforming section

1 Introduction

This document describes the usage of the reference Matlab code for processing the raw ADC data collected using TI 4-chip cascade EVM in TDM MIMO mode. Five sections are included.

- The second section introduces the antenna array configuration of TI 4-chip cascade evaluation board.
- The third section describes the two operation modes that is supported by TI cascade evaluation board: MIMO and TX beamforming
- The fourth section describes the antenna calibration procedures in the two different modes. Specifically, how to generate a board specific antenna calibration matrix is discussed and how to apply the calibration matrix at runtime.
- The fifth section describes the performance characterization of both MIMO and TX beamforming operation.
- The sixth section describes the signal processing chain provided this reference Matlab code for MIMO operation.
- The seventh section describes the signal processing chain provided this reference Matlab code for TX beamforming operation.
- The eighth section illustrates the indoor test results using TI 4-chip cascade radar.
- The ninth section illustrates the outdoor test results using TI 4-chip cascade radar.

2 Antenna Array

Fig 1 shows the antenna array on TI 4-chip cascade evaluation board with one master device and three slave devices, with 12 TX channels and 16 RX channels. Among the 12 TX channels, the three TXs (TX1/2/3) from the master device is placed in the vertical direction for elevation antenna estimation. The remaining 9 TXs (TX4~TX12) and all 16 RX channels are placed in the horizontal plane for azimuth angle estimation. The relative distances between TXs and between RXs are shown in Fig 2. The three elevation antennas are placed to form a minimum redundancy array [ref1.] to improve elevation angle resolution. Every two azimuth TXs are spaced 2 wave length apart. RX array A and RX array C are placed 16-wavelength apart. RX array C and RX array B are placed four-wavelength apart. The virtual array in MIMO mode is shown in Fig 3, with 86 virtual antennas in azimuth direction. The overlapped antenna in azimuth is not shown in the figure. The elevation angle resolution is equivalent to the resolution achieved with 7 antennas.

TI 4 chip cascade EVM can also be used in two chip cascade mode with 6 TX and 8 RX channels highlighted in Fig 2. Fig 4 shows the virtual MIMO array in 2- chip cascade mode using TX ID of [1 2 3 10 11 12] and RX ID of [4 3 2 1 16 15 14 13], with 23 azimuth antennas and same elevation configuration with 4-chip cascade. Users can also use any subset of the antennas to form a virtual array. For example, when 9 TX with channel ID of [1 2 3 4 5 6 8 10 12] and all 16 RX are used, the corresponding virtual array is shown in Fig 5. In this example, the azimuth array has holes, which can cause higher side lobes in the angle spectrum. Some phase interpolation method can be applied to lower the side lobe level.

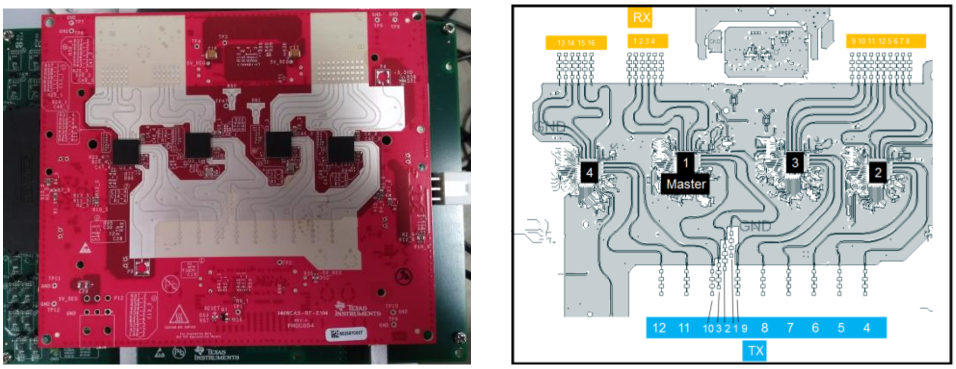

Fig 1: TI 4-chip EVM

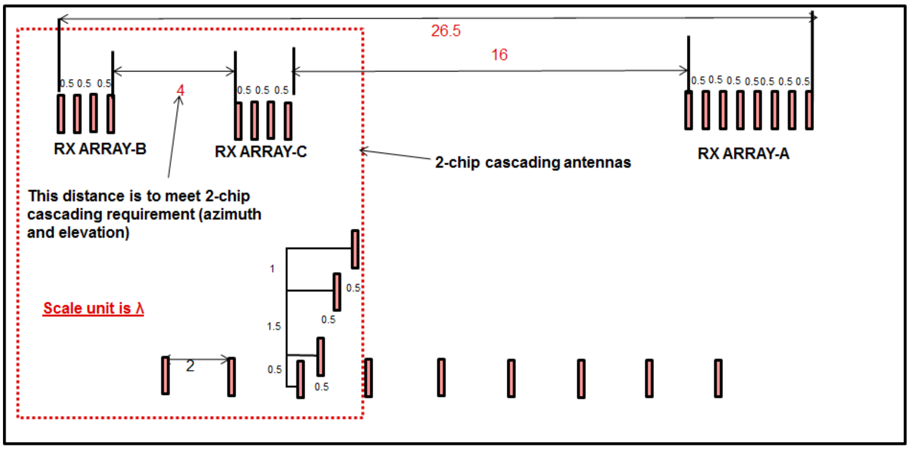

Fig 2: Antenna array positions

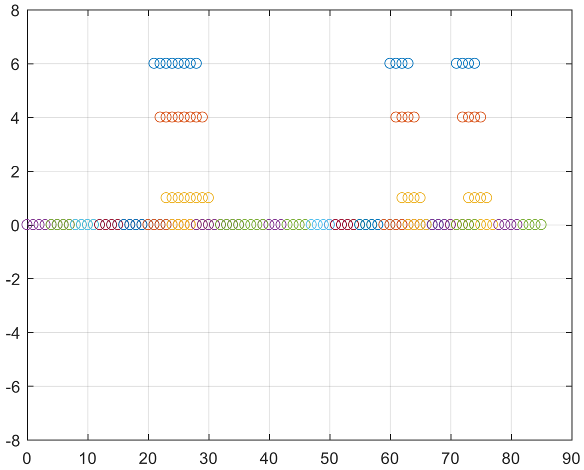

Fig 3: TI 4-chip cascade virtual MIMO array with 12 TX and 16 RX

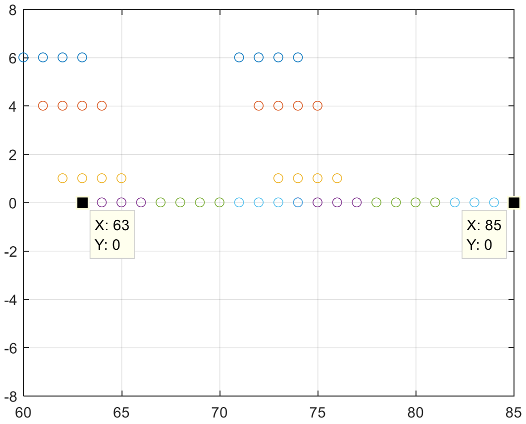

Fig 4: TI 2-chip cascade virtual MIMO array

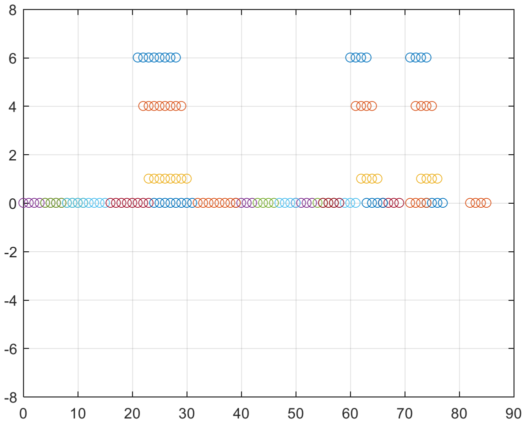

Fig 5: MIMO virtual array with 9TX and 16 RX

3 Two Operation Modes

TI 4-chip cascade board supports both MIMO and TX beamforming to achieve different functionalities.

3.1 MIMO Mode

In the MIMO mode, TX channels are transmitting independently to formulate a large virtual array to achieve high angle resolution. As shown in Fig5, the maximum achievable virtual array in MIMO mode is 86 channels. The orthogonality between all TX channels can be achieved by using either time duplex multiplexing or orthogonal binary sequences. The example provided in this document is based on time duplex multiplexing.

3.2 TX Beamforming Mode

In the TX beamforming mode, multiple TX channels are transmitting simultaneously and coherently to achieve higher gain/longer range in the main focused field of view. As shown in the following Fig 6, each TX channel of each device has a 6-bit configurable phase register with a step size of 5.625 degrees. The value of the phase value programed to each TX channel is calculated based on where the main beam should be focused. Since only 9 TX channels are placed at the same azimuth plane on TI 4-chip cascade board, these 9 TX channels can be used to steer the beam. Due to the coherent gain achieved in TX beamforming mode, its detection range is much longer than that achievable in MIMO mode.

Fig 7 shows the comparison between MIMO and TX beamforming modes in terms of gain. The gain achieved in MIMO is linearly proportional to the number of TX channels, as opposed to squared proportional in TX beamforming mode.

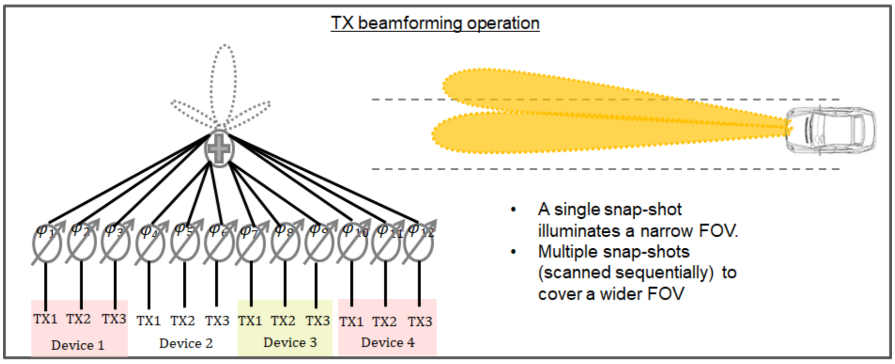

Fig 6: TX beamforming operation

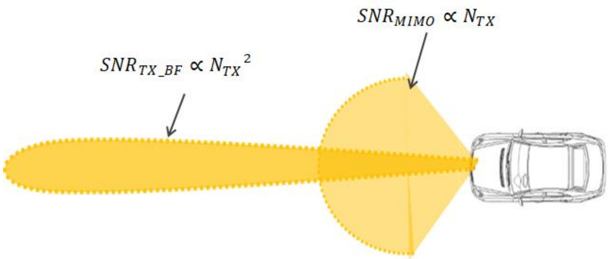

Fig 7: Gain comparison of MIMO and TX beamforming operations

3.2.1 Phase value calculation for beamforming

The amount of phase value to be programed to each TX channel is computed as a function of array factor and target angle. Assuming N TX channels, with TX1 as a reference, the distance between every other antenna and TX1 is the known distance when the antenna array is designed during board development. For TI cascade EVM, the distance between every two adjacent two TX channels is twice of the wavelength.

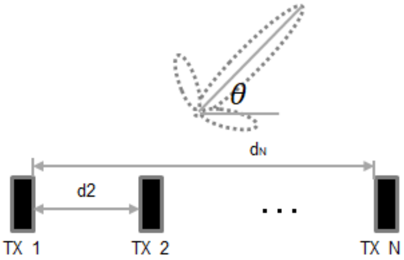

Fig 8-1: TX array for beamforming

Given the notation in Fig 8-1, the phase value for each TX channel is calculated as:

$$\vec{\emptyset} = [\emptyset_1\ \emptyset_2\ \emptyset_3\ \dots\ \emptyset_N] = [0\quad 2\pi\frac{d_2}{\lambda}\sin\theta\quad 2\pi\frac{d_3}{\lambda}\sin\theta\quad \dots\quad 2\pi\frac{d_N}{\lambda}\sin\theta]$$

The ideal phase value is further quantified by the allowed phase step size of 5.625 degree to calculate the integer value to be programed to the registers (TX calibration phase value will also be added as shown in the next section).

$$\overrightarrow{\emptyset_{int}} = \lfloor[\emptyset_1\ \emptyset_2\ \emptyset_3\ \dots\ \emptyset_N]/5.625\rceil$$

As an example, for TI cascade EVM, 9 azimuth TX antennas can be used for beam steering, with $[d2 = 2\lambda,\ d3 = 4\lambda, \dots, d9 = 16\lambda]$. If the desired steering angle is 30 degrees, then the phase vector is as shown below in degrees.

$$\vec{\emptyset} = \frac{[0\quad 4\pi\sin 30^o\quad 8\pi\sin 30^o\quad \dots\quad 32\pi\sin 30^o]}{\pi} * 180$$

The TX beamforming application supports both chirp based beam steering and frame based beam steering. Advanced frame configuration is used for either case.

- Chirp based beam steering

In the subframe used for TX beamforming, the number of chirps used in this subframe is equal to the number of different desired angles. Each chirp configuration is associated with phase values for the TX array, calculated based on the corresponding desired steering angle. Within a burst, all chirp configurations are looped over till the end of the burst. Fig 8 -2 demonstrates the mechanism of chirp based beam steering.

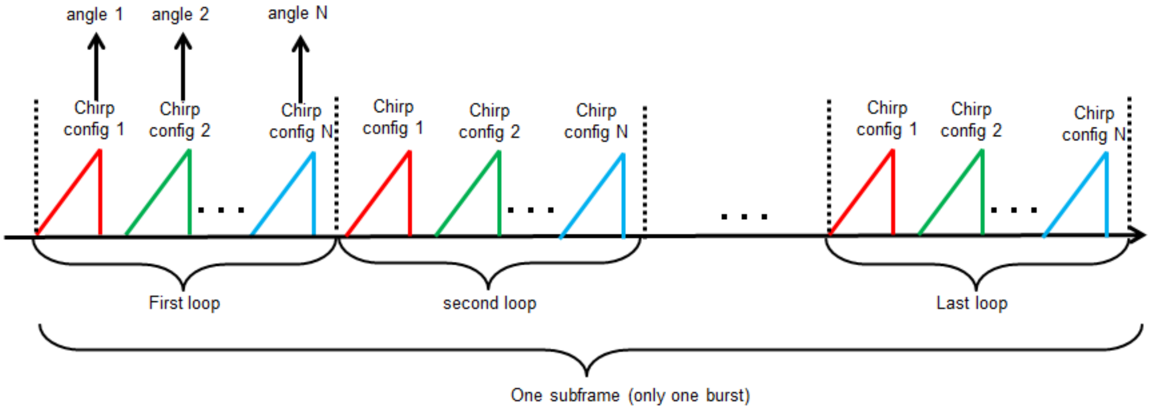

Fig 8-2: chirp based beam steering

- Burst based beam steering

In the subframe used for TX beamforming, the number of chirps used in this subframe is equal to the number of different desired angles. Each chirp configuration is associated with phase values for the TX array, calculated based on the corresponding desired steering angle. The number of burst within this subframe is equal to the number of different desired angles (same as number of chirp configurations). Each burst is associated with each chirp configuration, so a burst is equivalent to a frame within which each chirp has the same phase shifter value. Fig 8-3 demonstrates the mechanism of chirp based beam steering.

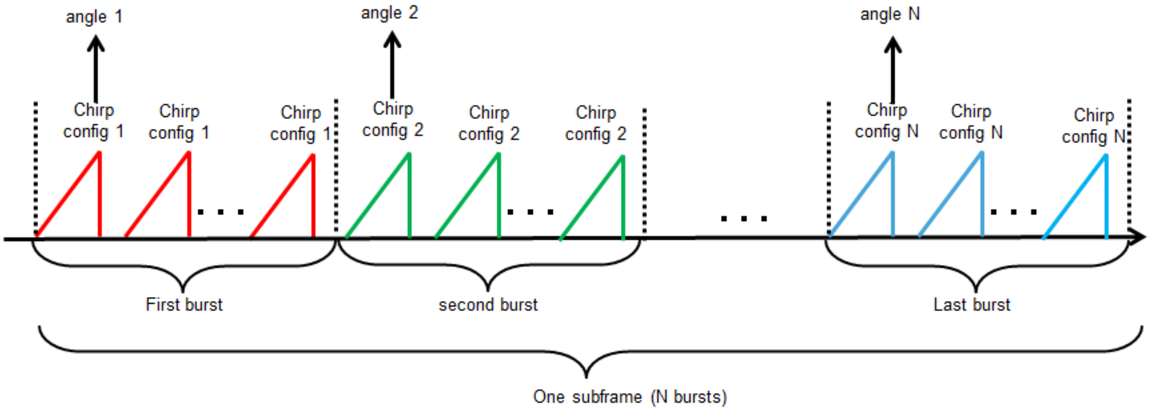

Fig 8-3: frame based beam steering

4 Antenna Calibration

Antenna calibration is to estimate the frequency, phase, amplitude mismatch across one master device and three slave devices. The mismatch can be caused by various reasons, such as path length mismatch, chip to chip variation, antenna coupling, etc. The frequency mismatch is usually minimized by routing path length match during the board layout stage. The calibration method proposed by TI reference design is a one-time bore side calibration method. It is suggested to perform board specific calibration to achieve best angle performance.

4.1 How to generate calibration matrix

To generate a calibration matrix, it is suggested to put a corner reflector at distance of 5 meters and beyond, with a typical corner reflector RCS of 1~2 square meters, as shown in Fig. 9. The corner reflector should be aligned with the array center of board in both azimuth and elevation direction. A level sensor with laser pointer can be used for alignment.

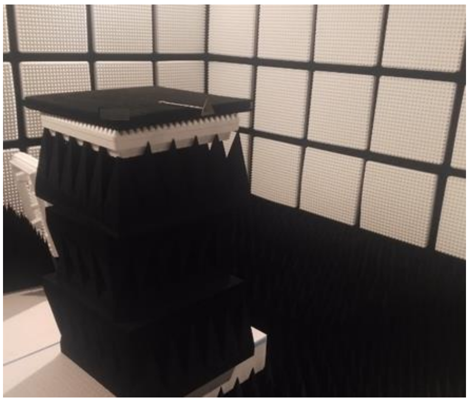

Fig 9: antenna calibration set up with corner reflector

Once the corner reflector is placed at the center position, a few frames of raw ADC data needs to be collected by using the example script provided in the Radar Studio release. During the data collection, turn on 12 TX in a TDM MIMO mode and all 16 RX channels are on at the same time.

After data collection, user can run the example antenna calibration code to generate the calibration matrix. The calibration matrix generation follows the sequence described by Fig 10. After the raw binary data is read and formatted so that data from 192 virtual channels are separated. Range FFT is performed on each channel and the peak corresponding to the corner reflector is identified as the local maximum within in [D-1 D+1] meters, where D is the approximate target range provided by user. The FFT peak index from all 192 channels form a matrix size of 12 x 16, which will be used for frequency calibration step. The complex values at the peaks from all 192 channels form a complex calibration matrix of size 12 x 16, which will be used for phase and amplitude calibration. These two matrixes are saved to a mat file to be loaded when applying the calibration results to the ADC data.

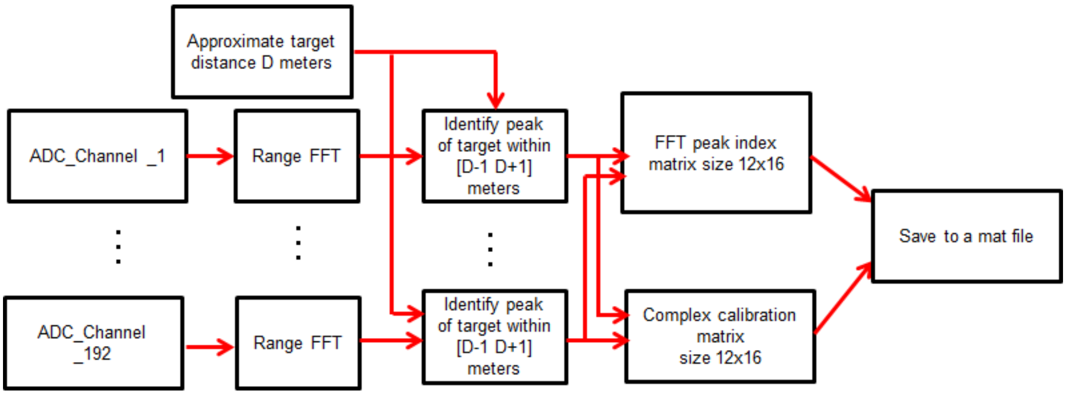

Fig 10: Flow to generate calibration matrix

4.2 Apply calibration matrix in MIMO operation

The saved calibration information is applied to the raw ADC data collected in MIMO mode in two steps on the flow shown on Fig 11.

- **First step: frequency calibration**

  The FFT index of TX1/RX1 channel is used as reference that is compared with all the other 191 channels. The FFT index difference and chirp parameters are used to compute the frequency calibration vector using the following equation.

$$\vec{F} = 2\pi \times \Delta P \times \frac{f_{chirp}}{f_{calib}} / (N \times I_{interp}) \times \vec{n}$$

  ΔP is the FFT peak index difference for a virtual channel; f_{chirp} is the FMCW chirp frequency slope; f_{calib} is the FMCW chirp frequency slope used for calibration which can be different from f_{chirp}; N is the number of ADC samples per chirp; $\vec{n}$ = [0 N-1] is the ADC sample index; I_{interp} is the interpolation factor used for frequency calibration that is further explained in the next section. $\vec{F}$ is the computed frequency calibration vector.

$\exp(-j \times \vec{F})$ is multiplied with the raw ADC data for frequency calibration. For each virtual channel, $\vec{F}$ is calculated and applied to the corresponding ADC data.

- **Second Step: phase and amplitude calibration**

  After frequency calibration, the phase and amplitude calibration value is calculated based on the complex value of the reference channel

$$C_{ph\_am} = C_{ref}/C_{txi/rxj}$$

  C_{ref} is the complex value of reference channel, $C_{txi/rxj}$ is the complex value of other channels; C_{ph_am} is the calculated phase and amplitude calibration value. C_{ph_am} is 1 for reference channel and different for every other channel. C_{ph_am} is multiplied with the output from the frequency calibration and the result is the final calibrated ADC data.

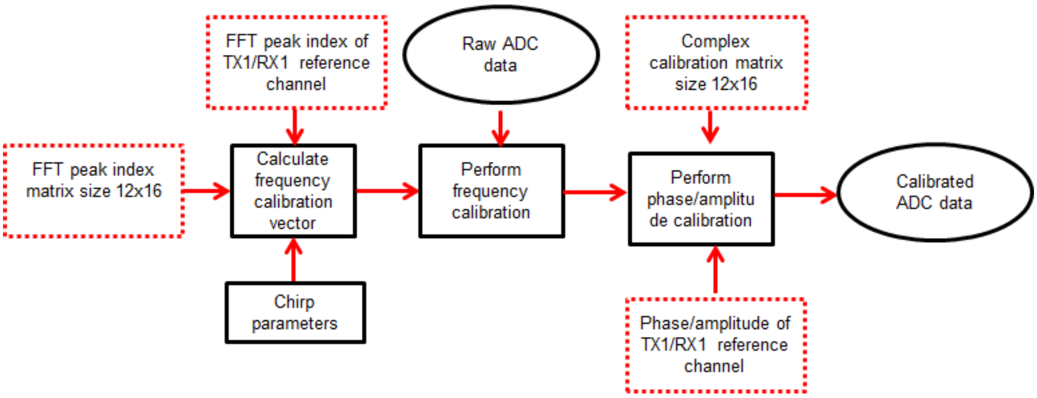

Fig 11: Flow to apply calibration matrix to ADC data

4.3 Apply calibration matrix in TX beamforming operation

The saved calibration information is applied in TX beamforming operation as shown in Fig 12. The phase value of the 12 x 16 complex value matrix obtained from Section 4.1 is averaged across the 16 RX channels to obtain a phase calibration vector for the 12 TX channels. According to the index of TX channel used in actual TX beamforming mode, the corresponding phase value within this 12x1 vector is used for the phase compensation. The compensation phase value together with the phase value calculated based on the desired steering angle (refer to Section 3.2.1) is used to program the phase shift register value before starting beam steering process.

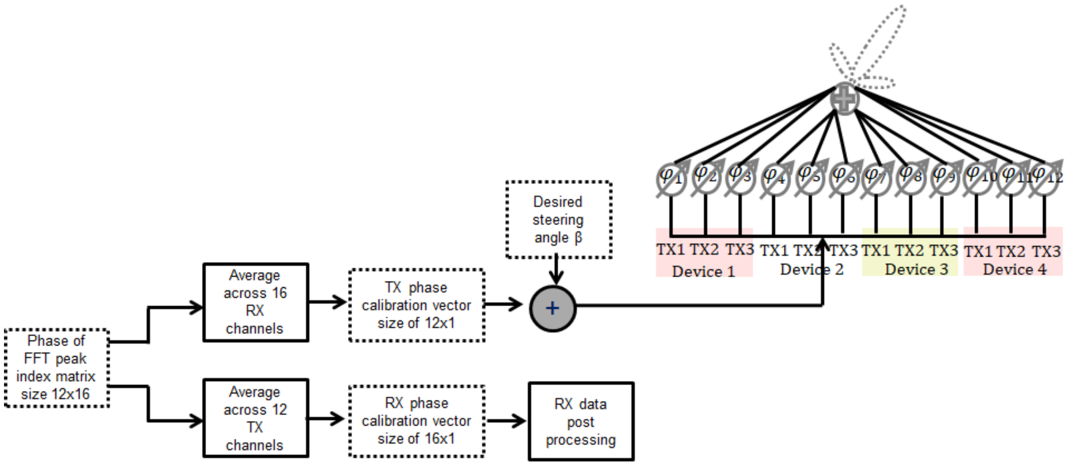

Fig 12: Apply calibration in TX beamforming mode

Similarly, the phase across the 12 TX channels is averaged to obtain a phase calibration vector for the 16 RX channels. This is phase only RX calibration assuming that there is no frequency mismatch across the 16 RX channels. The frequency mismatch across 16 RX channels can be captured by collecting calibration data by following these steps

1) Put a corner reflector at a known distance, for example, around 6 meters
2) Configure all TX channels to steer towards zero degrees
3) Check the FFT peak index of all 16 RX channels; the FFT peak index indicates the frequency mismatch, similar to the frequency mismatch described in the above MIMO calibration section.

The phase calibration value is applied during the RX data post processing stage. More details will be discussed in the signal procession section of TX beamforming.

5 Performance Characterization

This section discusses the performance characterization results conducted in the lab for the two different operation modes.

5.1 Performance characterization in MIMO operation

This section describes the performance characterization results in the MIMO mode. Specifically, the frequency mismatch, phase/amplitude mismatch, antenna pattern and angle estimation accuracy are discussed as below.

5.1.1 Frequency mismatch

For TI 4-chip cascade EVM, the frequency mismatch is measured to be less than one frequency bin size for a corner reflector at 5 meters in the bore side. Fig 13 shows the frequency synchronization across all 192 (12 x 16) virtual channels. The peak at range index 85 corresponds the corner reflector at 5 meters. All peaks occur at the same frequency indicates the good synchronization across all 192 channels. To further check the frequency difference across all channels, zero padded FFT can be performed to improve the frequency accuracy, as shown in Fig 14. The frequency discrepancy starts to show up across the channels. The right sub figure of Fig 14 plots the range FFT peak index after zero padding. It shows that the peak index range from 320 to 324, with maximum difference of 4. By default, the provided Matlab calibration code utilizes 5 times interpolation for calibration matrix generation.

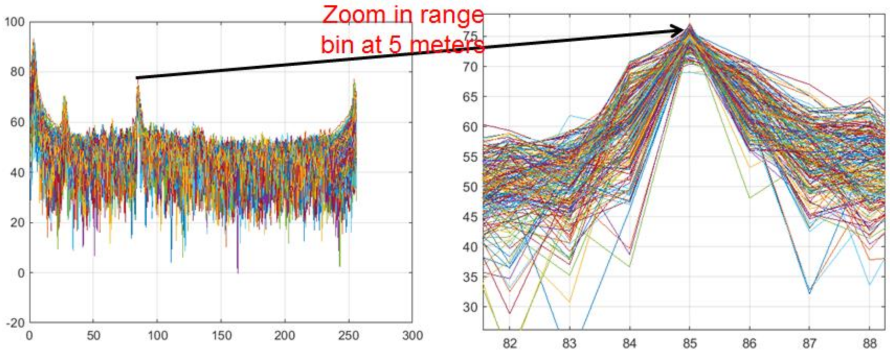

Fig 13: Range FFT profiles of all 192 channels (FFT size 256)

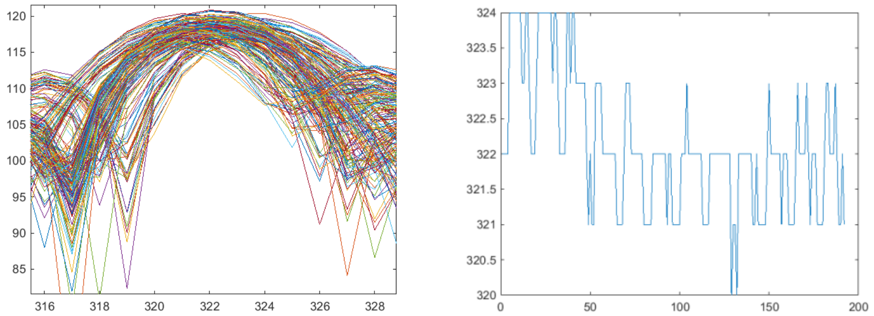

Fig 14: Zero padded range FFT profiles of all 192 channels (FFT size 256 x 5)

5.1.2 Phase/amplitude mismatch

Besides frequency mismatch, phase mismatch should also be compensated to achieve coherent processing across all the channels. Amplitude calibration is optional in the example Matlab code. Fig 15 shows the typical phase (top) and amplitude mismatch (bottom) at the bore side after comparing with the reference channel, with different color indicates different TXs. For each TX, the corresponding phase and amplitude value is shown for all 16 RXs. The phase mismatch and amplitude mismatch value is applied to the raw ADC data for calibration.

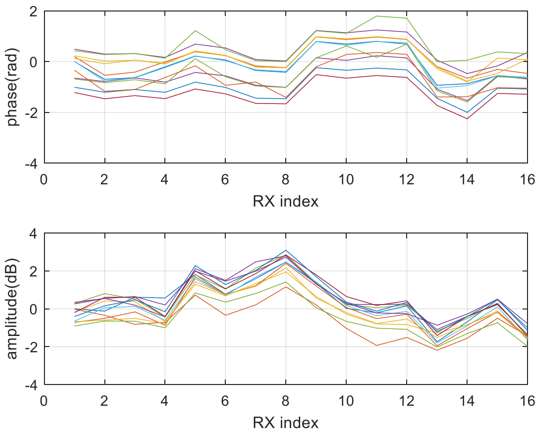

Fig 15: Phase and amplitude mismatch

5.1.3 RF frequency dependency

According to TI antenna calibration study, it is suggested that the calibration vector should be RF frequency dependent to achieve the best performance. In this study, ADC data is collected at 5 different RF frequencies: 76G~77G, 77G~78G, 78G~79G, 79G~80G, 80G~81G. The other chirp parameters are shown in below table.

Table 1: Chirp parameters for measurements

Chirp parameter	**Value**
RF start frequency (GHz)	different
Chirp slope (MHz/us)	25
Idle time (us)	5
TX start time(us)	0
ADC start time(us)	6
Ramp end time(us)	40
ADC sampling rate (MHz)	9
Number of samples per chirp	256
Chirps per frame	128

A rotation motor is used to rotate the radar within [-60 60] degrees with 5 degrees each step. There are total 25 measurements. ADC data is collected at each angle location. Phase mismatch and side lobe ratio in angle spectrum is examined with either a cross calibration matrix collected at zero degree of 76G~77G frequency or unique calibration matrix for its own RF frequency at zero degree.

Fig 16 shows the phase mismatch with a cross calibration matrix and a unique calibration matrix. The x axis is the azimuth virtual array channel ID. There are total 86 channels as described in Section 2. The y axis is the phase mismatch in degrees. The phase mismatch value is calculated as the phase difference between the measured azimuth array phase and the calculated ideal phase based on the antenna configuration. For 76GHz, it is the same as expected. For other RF bands, using a unique calibration matrix is always preferred.

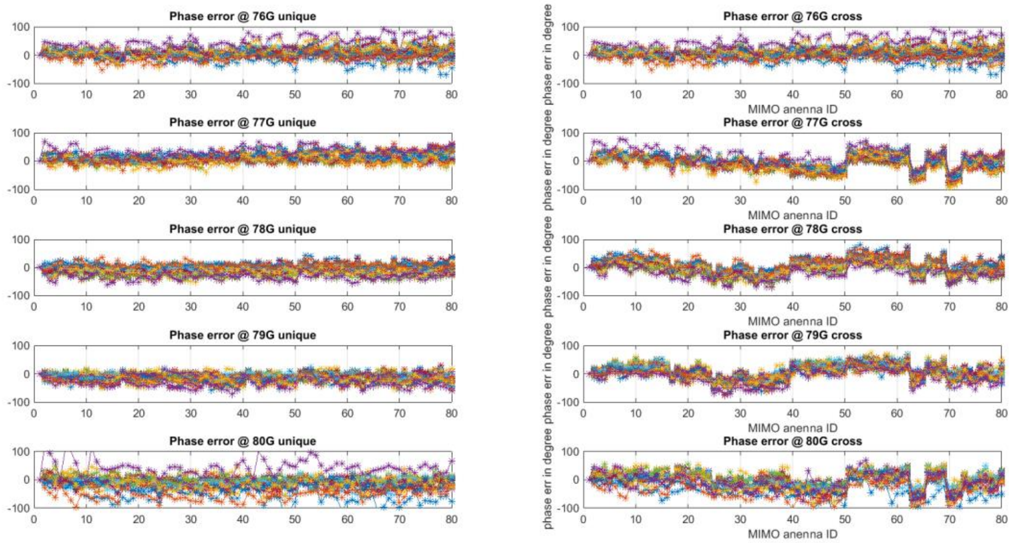

Fig 16: Phase mismatch across different RF frequency

Besides phase mismatch, peak to first side lobe ratio is also measured as defined in Fig 17. Fig 18 shows the peak to first side lobe ratio in terms of dB, comparing to the ratio of 76GHz. Therefore, it is all zero for 76GHz measurement. The higher the value is, the worse the angle spectrum performance. According to this study, it is suggested that the calibration vector should be RF frequency dependent to achieve the best performance.

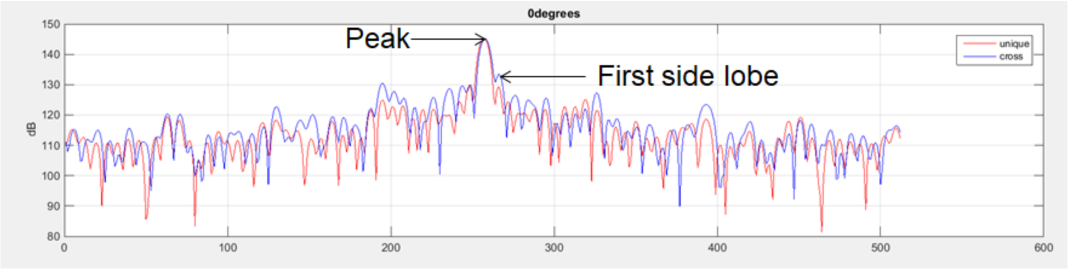

Fig 17: peak to first side lobe

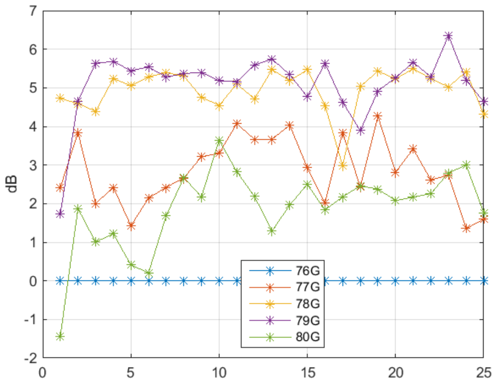

Fig 18: peak to first side lobe ratio

5.1.4 Antenna distance in angle estimation

The distance between antennas as shown in Section 2 is always scaled in terms of wave length which is RF frequency dependent. On the other band, the physical distance between antennas is fixed. As a result, the antenna distance value used in angle estimation needs to be scaled correctly. The following equation indicates how a phase at a certain antenna is usually calculated for a target at θ angle with d_i distance from the reference antenna. Normally, we assume d_i/λ is integer times of 0.5. To get accurate angle estimation, d_i/λ should be RF frequency dependent since the wave length changes at different RF frequency.

$$\emptyset_i = 2\pi \times d_i/\lambda \times \sin(\theta)$$

TI has tried the following 6 different RF frequency bands, the optimal d_i/λ value is suggested as in the table below. Fig 19 demonstrates the importance of using the right d_i/λ value to get accurate angle estimation. The left and right subplot shows the phase error and corresponding angle estimation error with and without the optimized d_i/λ value, respectively. The phase mismatch error and angle accuracy significantly improved by applying the adjusted d_i/λ value.

Table 2: suggested d_i/λ value for angle estimation

RF	**76~77G**	**77~78G**	**78~79G**	**79~80G**	**80~81G**	**77~80G**
d_i/λ	0.496	0.504	0.51	0.516	0.522	0.51

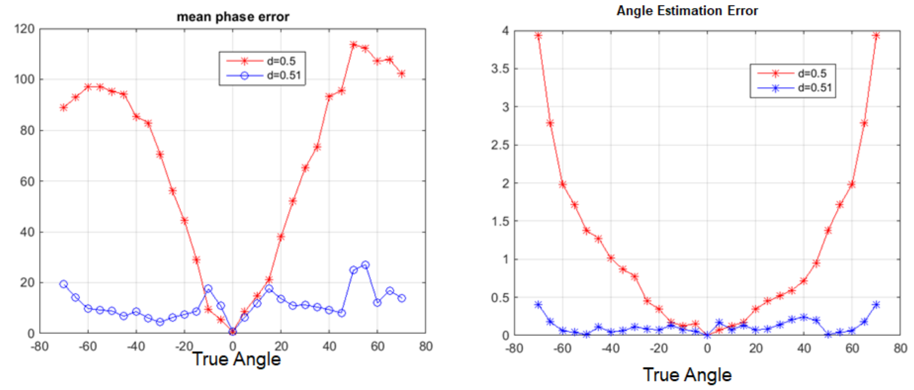

Fig 19: Phase mismatch and angle estimation error with different d_i/λ value

5.1.5 Antenna gain pattern and phase measurement

Antenna gain pattern and phase mismatch is also measured based on TI 4-chip cascade board. A rotation motor is used to rotate the radar within [-60 60] degrees with 5 degrees each step. ADC data is collected at each angle location. A corner reflector RCS of 1~2 square meters should be aligned with the array center of board in both azimuth and elevation direction. A level sensor with laser pointer can be used for alignment. Fig 20 is the sequence for antenna gain pattern and phase analysis. At each measurement angle, for each virtual channel, the ADC data is first calibrated with the calibration matrix gets at zero degree. Then range FFT is performed followed by peak detection corresponding to the corner reflector. The peak complex value is formatted as a 12 x 16 matrix. This sequence is repeated for each angle. After obtaining the complex matrix at each angle, the amplitude of the complex value is used for gain analysis and the angle is used for phase analysis.

Fig 21 shows the antenna gain patter at different RF frequency in the angle range of [-60 60] degrees in dB. The gain in this plot is averaged across 16 RX channels per TX. Different color indicates different TXs. Note that it is combined TX/RX gain after FFT processing, different from the definition of antenna gain at design phase. The highest gain is achieved at 76GHz and 77GHz, and deceases slightly as RF frequency increases. The difference between different color lines indicates the average RX gain difference when different TX is involved. This difference is within a few dB, which shows the gain consistency across all the antennas. Fig 22 shows the angle mismatch averaged across all channels at different measurement angle. The x axis is in true angle of rotator in the range of [-60 60] degrees. The y axis is angle error in degrees. Different color in this plot shows the phase error at different RF frequencies. The general, the phase error is below 50 degrees and increases as angle increases. This can be caused by SNR loss at large angles.

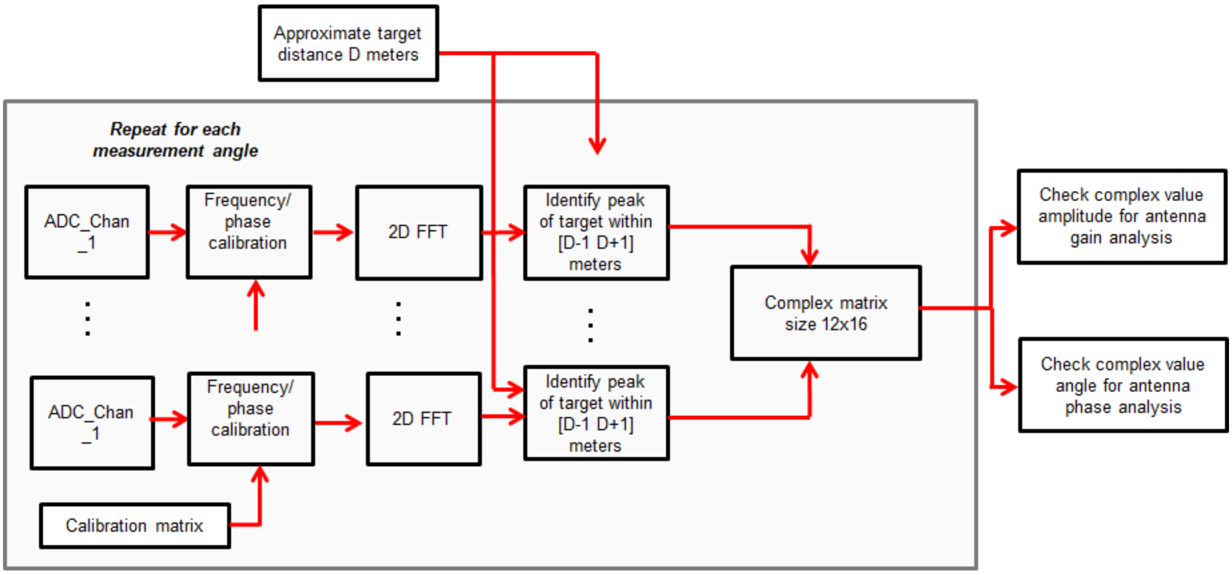

Fig 20: Antenna gain pattern and phase analysis

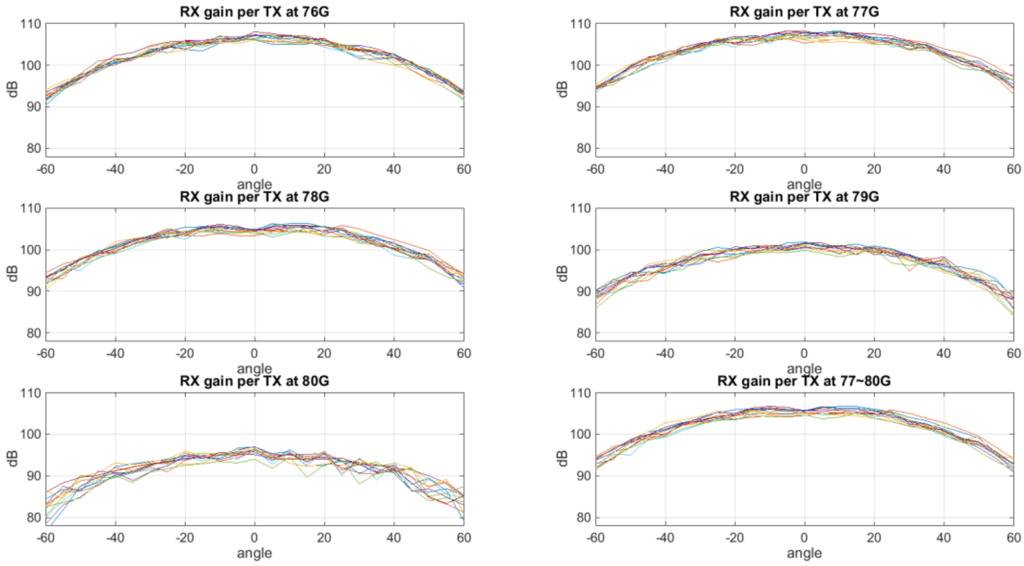

Fig 21: Antenna gain pattern of TI cascade board

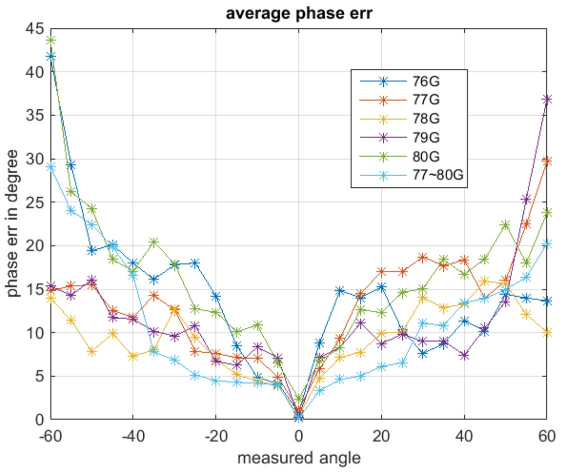

Fig 22: Antenna phase mismatch of TI cascade board

5.2 Performance characterization in TX Beamforming operation

This section describes the performance characterization in TX beamforming mode. Specifically, TX beamforming gain results and TX beamforming beam pattern are discussed as below.

5.2.1 TX beamforming gain

Fig 23 is the actual experimental results for the gain improvement with different number of TX channels on simultaneously. The expected gain with 9 TX channels in the same azimuth direction is around 20*log10(9) = 19.1dB. The measured gain is around 20dB, close to the expected gain. The 1dB difference might be caused by the reflection fluctuation.

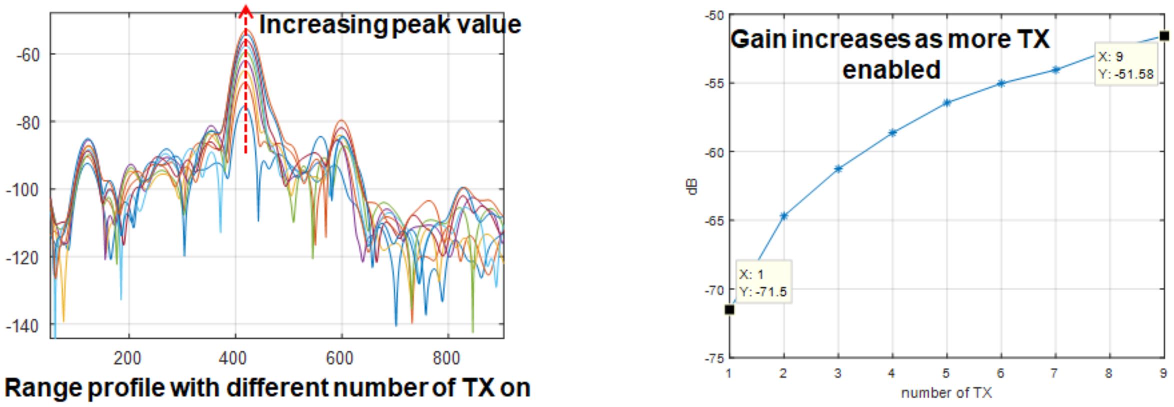

Fig 23: Gain comparison of MIMO and TX beamforming operations

5.2.2 Beam pattern measurement

To measure how accurate the beam is actually steering towards the target, a beam pattern measurement experiment is carried out. In this test, a rotation motor is used to rotate the radar within [-60 60] degrees with 1 degrees each step. During each rotation circle within 120 degrees, the TX beam is constantly steering towards a defined angle. Seven steering angles are tested: [-15 -10 -5 0 5 10 15]. Therefore the motor rotates seven times. ADC data is collected at each angle location. A corner reflector RCS of 1~2 square meters should be aligned with the array center of board in both azimuth and elevation direction. A level sensor with laser pointer can be used for alignment.

Fig 24 shows the process of generating beam pattern in TX beamforming mode. Each frame received from each RX channel is performed range and Doppler FFT. Identify the peak corresponding to the range of corner reflector in the range direction on the zero Doppler bin. The amplitude of the 16 identified peak values are averaged as the estimated signal reflection level at the give angle. This process is repeated for each angle within [-60 60] degree with 1 degree each step and the result is the beam pattern for a given steering angle. The out loop repeats for each of the test steering angles.

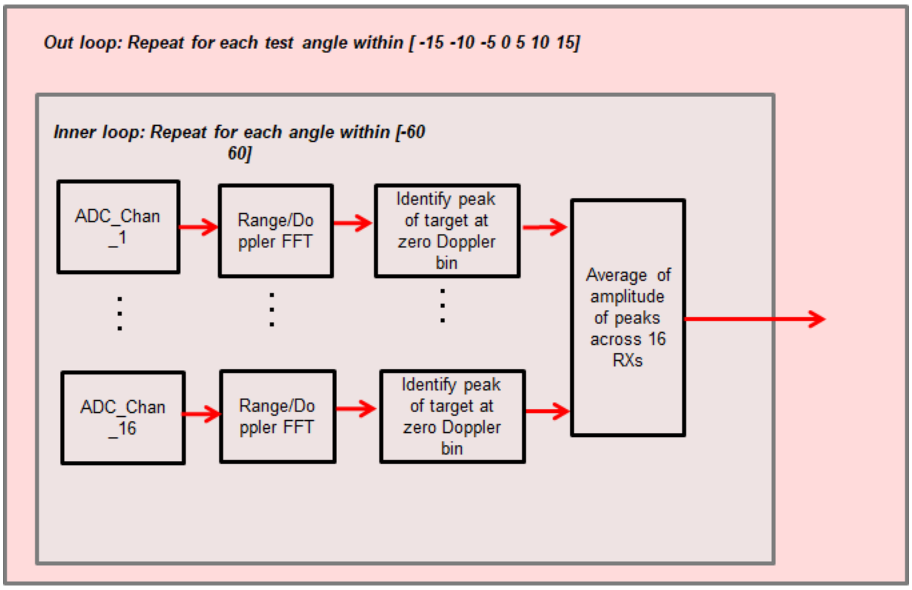

Fig 24: Beam pattern measurement in TX beamforming mode

Fig 25 shows the resulted beam pattern for 7 different steering angles. The highlighted peak shows the peak angle when the beam is steered towards the target. As an example, if beam is steering towards -15 degree, the reflection peak occurs after the motor rotates by 15 degrees in the opposite direction when the main beam lobe is directly towards the target. Similarly, the peaks of the other 6 test angles are also identified in Fig 25 with around 1 degree offset. The grading lobes on each plot are caused by the adjacent TX antenna distance being two wavelengths. These grading lobes can be canceled by RX beamforming, as demonstrated in the next section.

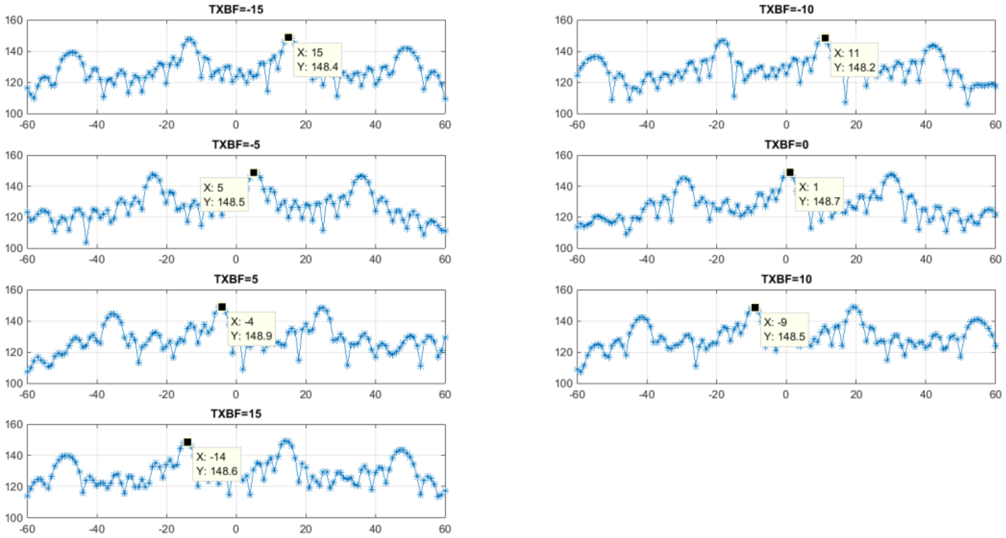

Fig 25: Beam pattern measurement results with different steering angles

6 Signal Processing Chain in MIMO Mode

The raw signal collected in MIMO mode is processed in a flow as shown in Fig 26 as an example.

- **ADC data read and calibration**

After each data collection, a binary data file and the corresponding chirp configuration parameters are saved. These two files are the inputs to the ADC data read and calibration module. The binary data file is read/parsed according to the chirp parameters based on the data format, samples per chirp, chirps per frame, number of TX/RX channels. Then the data is reformatted into a 4D matrix, with the dimension of samples per chirp, chirps per frame, number of RX channels, and number of TX channels. Each of the TX/RX channel is calibrated according the pre-calculated calibration matrix that can be obtained using the procedures as described in Section 3.

- **Range/Doppler FFT**

For each TX/RX channel, range FFT is performed followed by Doppler FFT. The default windowing is hanning window. The FFT size is determined as the closest integer that is power of 2.

- **Detection**

The output of range/Doppler FFT is sent to the detection module. The first step is non-coherent integration across all the virtual channels. The integration output goes through the CFAR detection step that does 1D range CFAR detection followed by 1D Doppler CFAR detection at the detected range bins. For each cross detected range/Doppler point, the maximum velocity extension algorithm is applied to correct any possible velocity ambiguity caused by TDM MIMO. The recovered velocity is used to correct the phase jump that is again caused by the TDM MIMO for each detected point. The details of maximum velocity extension and phase compensation will be discussed in a separate section.

- **Angle estimation**

For each detected point, angle estimation is performed based on the signal vector with corrected phase. If the configured array is azimuth direction only, only azimuth angle estimation is needed. If a 2D configured array is involved, both azimuth and elevation angle estimation is performed. Note that multiple angles will be detected in the azimuth direction, but only the maximum peak is selected in the elevation direction.

- **GUI**

The output of angle estimation is a point cloud. Each point provides information of range, velocity, azimuth and elevation (if available). The content of GUI is TBD.

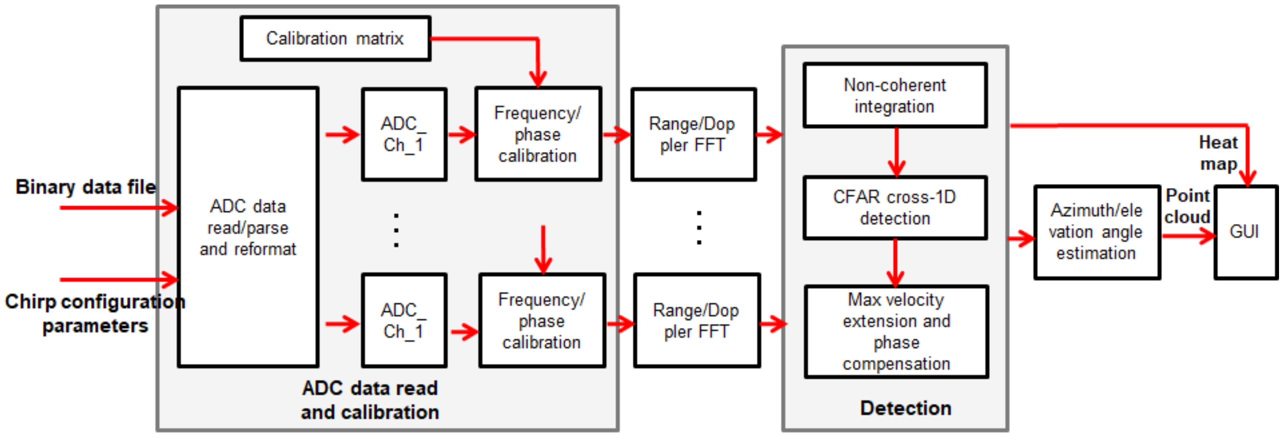

Fig 26: Signal Processing Flow for MIMO

7 Signal Processing in TX beamforming Mode

This section provides an example signal processing chain in TX beamforming mode. Users might have their own preferred signal chain depending on the application. This example signal processing chain is used to generate an azimuth/range heat map by stitching multiple TX beamforming scans together.

Fig 27 shows the block diagram of the example signal processing chain in TX beamforming mode. The desired steering angles are defined as [β1 β2 … βn]. For each angle βi, the phase shifter value is calculated based on the TX phase calibration vector and βi with given TX antenna positions (refer to Section 3.2.1). The received ADC data from each RX channel goes through range and Doppler FFT, and only zero Doppler bin is selected for range/azimuth heat map generation assuming it is a static test scene. For moving test scene, user needs to change accordingly. For each range bin at zero Doppler, after phase compensation using calibration vector, RX beamforming is performed to steering the RX beam towards the same βi where the TX channels are focusing on. As a result, one range line is generated for each angle βi. By stitching all the lines generated with different βi angles, a range/azimuth heat map is generated.

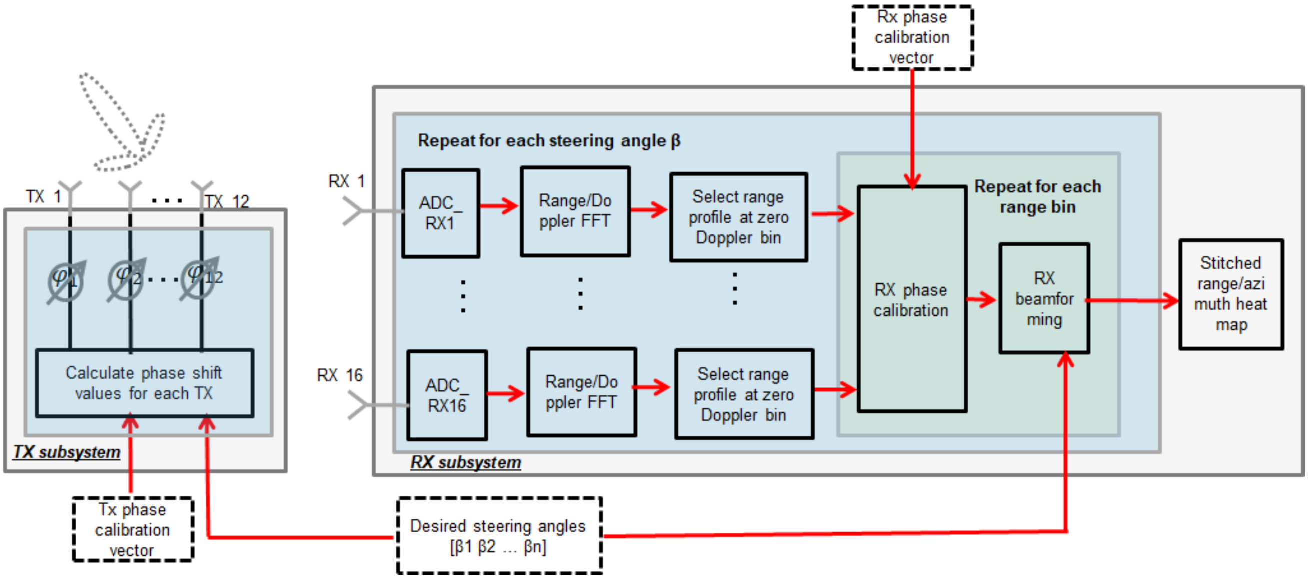

Fig 27: Example signal processing chain for TX beamforming mode

Fig 28 shows the example heat map results. Two corner reflectors are separated by around 1.8 degrees at 6 meters within the anechoic chamber. The anechoic chamber size is around 6 meters in width and 12 meters in length. The radar is put around 4 meters away from one side. The top left and top right plots are the heat map results (top-down view) running in MIMO mode and stitched TX beamforming mode. The TX beam is steering within [-60 60] with step size of 0.5 degree. The rectangular shape corresponding to the anechoic chamber wall, and the two bright spots in the middle are corresponding to the two corner reflectors. The bottom left and bottom right plots are the heat map results in a 3D view, with the height indicates the reflection intensity. The separation of the two peaks is more visible in the 3D view. It is worth to note that the grading lobes caused by the wide distance of adjacent TX channels are no longer observed because of the cancellation in the RX beamforming process.

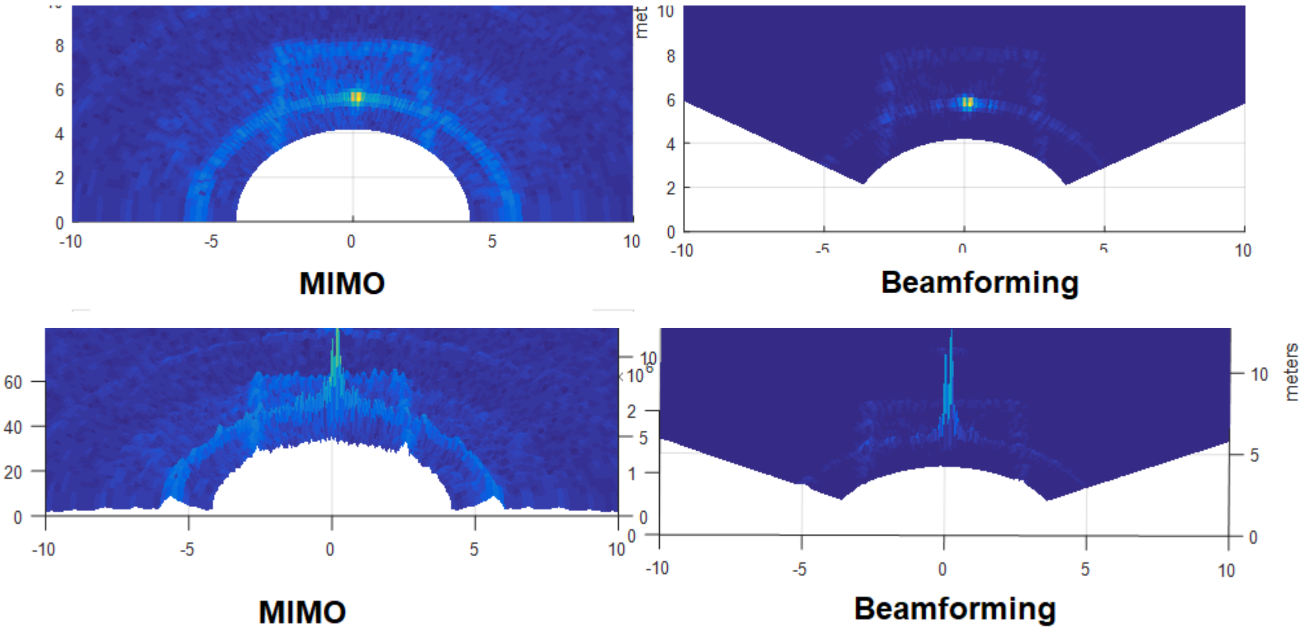

Fig 28: Comparison of MIMO and stitched TX beamforming

This experiment result proves that the receiver angle resolution in these two operation modes are equivalent since the effectively aperture size is the same. Further, the signal SNR in the beamforming is much higher due to the coherent gain in TX beamforming mode. The SNR in MIMO mode can be improved by increasing the chirp integration time.

In real application, it is not necessary to scan such a wide angle range, especially for long range application. User can scan a much narrower field of view as desired. The right subplot in Fig 29 shows the results when TX beamforming is scanning within [-10 10] degrees. The left corresponding MIMO picture is also shown as reference.

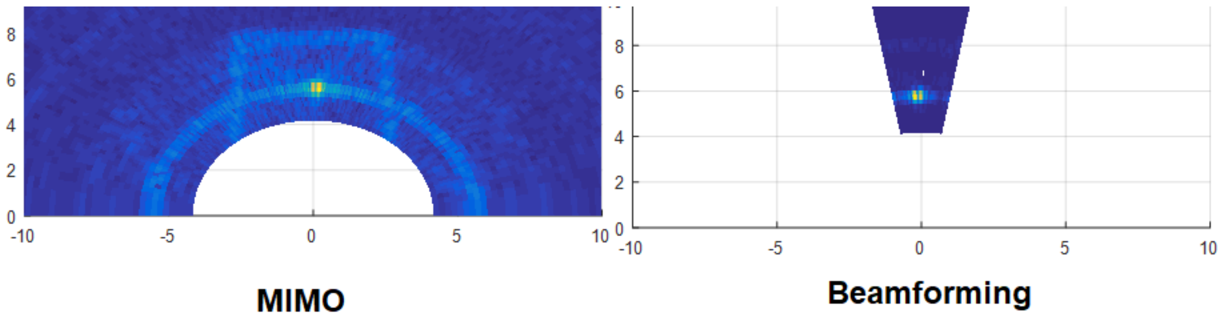

MIMO

Beamforming

Fig 29: Comparison of MIMO and stitched TX beamforming for narrower field of view

8 Indoor Test Results

This section describes the test results obtained within anechoic chamber. The measurements cover noise floor, angle estimation accuracy, and angle resolution.

The following table shows the chirp configuration used in the measurement.

Table 3: Chirp parameters for measurements

Chirp parameter	**Value**
RF start frequency (GHz)	77
Chirp slope (MHz/us)	79
Idle time (us)	5
TX start time(us)	0
ADC start time(us)	6
Ramp end time(us)	40
ADC sampling rate (MHz)	8
Number of samples per chirp	256
Chirps per frame	128

- **Noise floor measurement**

The following figure shows the noise floor measurement by facing the EVM towards the wall of anechoic chamber. Fig 30. on the right is the range spectrum. The x axis is the range FFT index, and the y axis is the signal strength in dB. Different color corresponds to 16 RX different channels. The noise floor is very flat at the range bins without reflecting target.

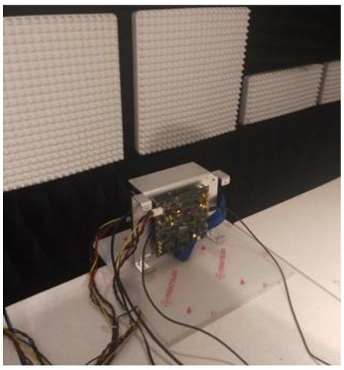

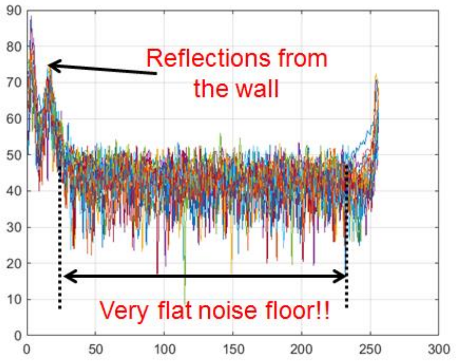

Fig 30: Noise floor measurement

- **Angle estimation accuracy measurement**

As described in the previous section, to perform angle estimation accuracy measurement, a rotation motor is required to rotate the radar within [-60 60] degrees with 5 degrees each step. ADC data is collected at each angle location. A corner reflector is placed at around 6 meters with RCS of 1~2 square meters. The corner reflector should be aligned with the array center of board in both azimuth and elevation direction. The antenna calibration method is Section 3 is applied before angle estimation. Fig 31 shows the angle estimation error at different RF frequency. The error is below 0.5 degree in average with maximum error less than 1 degree.

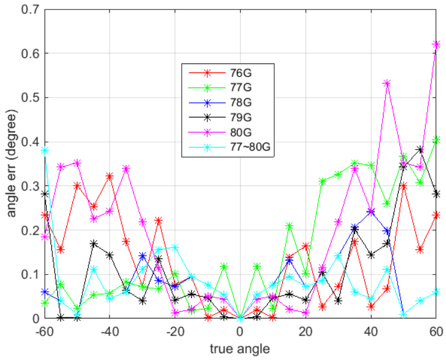

Fig 31: Angle estimation error at different RF frequency

- **Angle resolution measurement**

The angle resolution is performed with two corner reflectors placed at 5 meters with 1.7 degrees angle separation as shown in Fig 32. The two corner reflectors have respective peak RCS of 0.4 and 1.6 square meters. Fig 33 shows the angle resolution test results. The range profile shows that the target occurs at 5 meters. The angle spectrum shows the two peaks of the two corner reflectors with amplitude difference caused by RCS difference. The theoretical angle resolution with 86 virtual antennas is 1.4 degrees in the bore side.

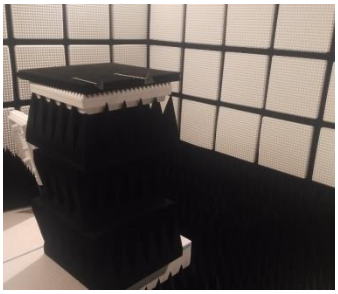

Fig 32: angle resolution test set up

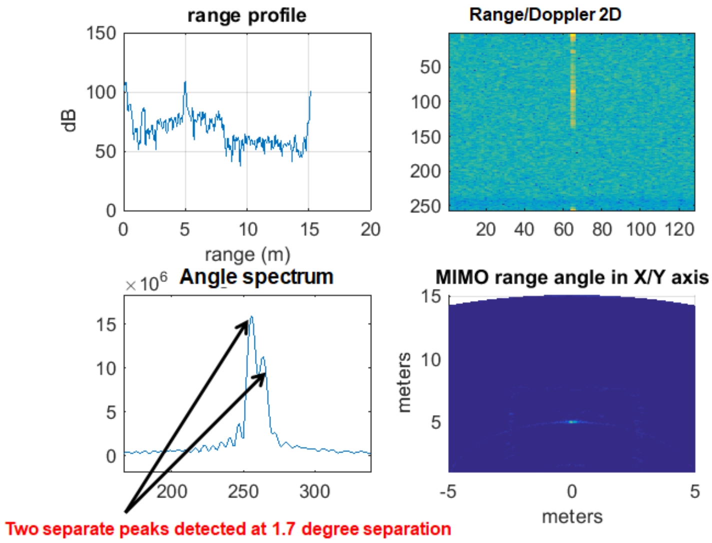

Fig 33: angle resolution test result

9 Outdoor Test Results

Outdoor tests also constructed as shown in this section, including detection of pedestrians and cars.

- **Detection and separation of multiple pedestrian**

  In this test, three pedestrians are walking closely side by side with similar velocity. The sensor is running in 9TX MIMO mode. To detect and separate the pedestrians requires high angle resolution since targets are in the same range and velocity. Results are shown in Fig 34. The range profile shows the detected points at the CFAR process. Those points are further processed in the angle of estimation step to generate the 3D point cloud. The three pedestrians are clearly separated. The corresponding point cloud is also shown using a single chip device, which fails to differentiate the three targets.

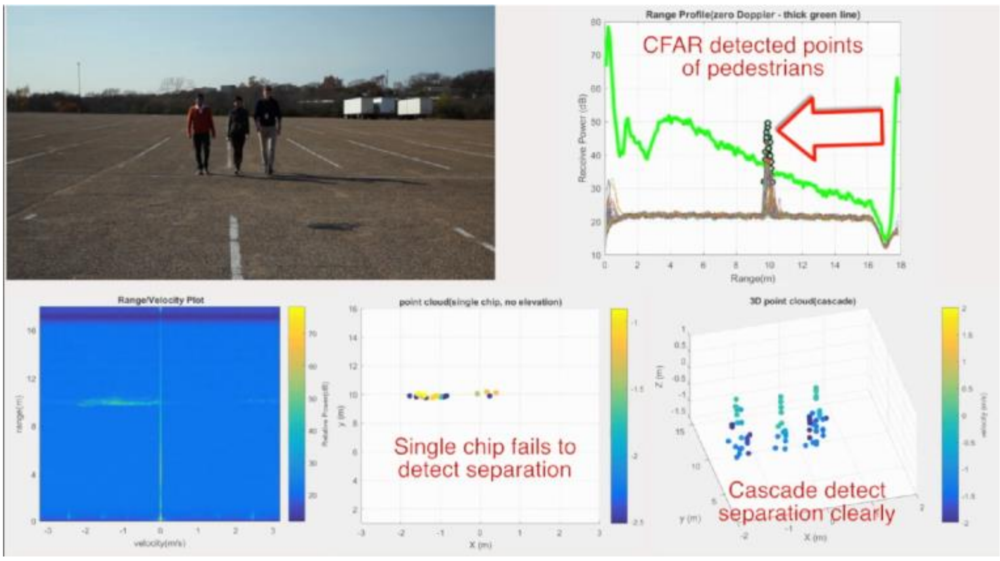

Fig 34: Detection and separation of multiple pedestrians

- **Detection and separation of adjacent cars**

In this test, two cars are driving on two adjacent lanes starting from 60 meters, with same range and velocity. The sensor is running in 9TX MIMO mode. Results are shown in Fig 35. The light pole, truck container and two cars are detected respectively. Some other targets are also detected, but not captured by the camera picture due to limited lens field of view. The cascade radar can clearly separate the two cars as shown in both the range/azimuth heat map and the point could.

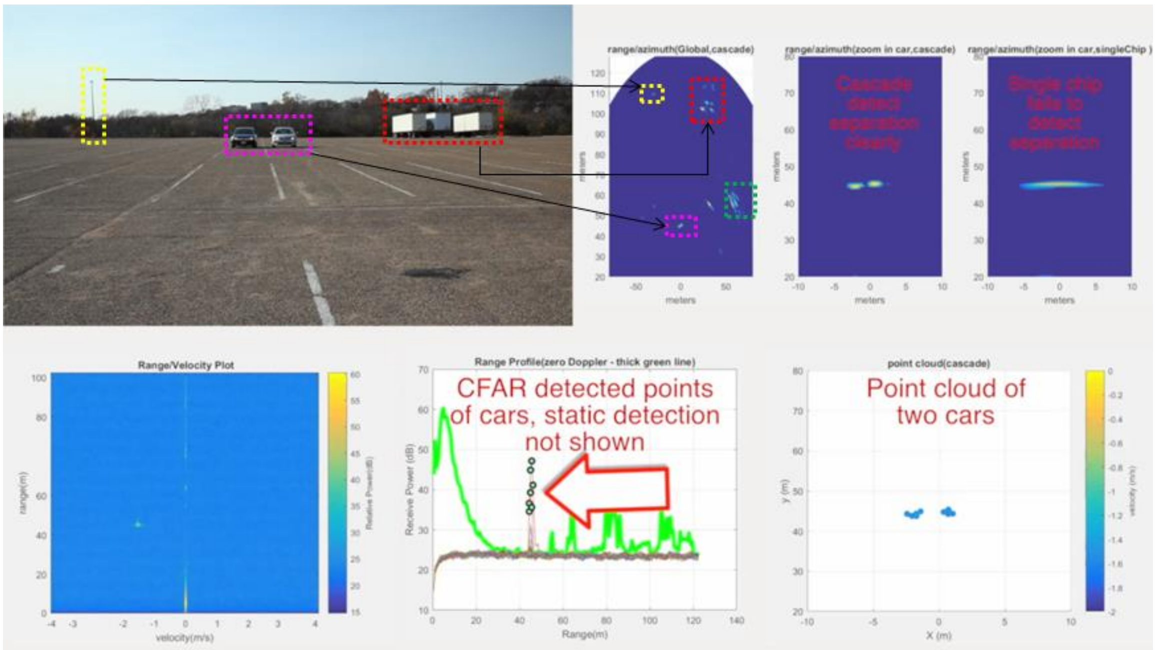

Fig 35: Detection and separation of adjacent cars

- **Detection of pedestrian beyond 120 meters**

In this test, the maximum detection range of a pedestrian is demonstrated by running 9TX beamforming. Results are shown in Fig 36. The pedestrian runs from one end of the parking lot to the other end, with total length around 150 meters. A drone is hovering to take the image. The following picture shows that the pedestrian is still detected at 120 meters with SNR of 15 dB.

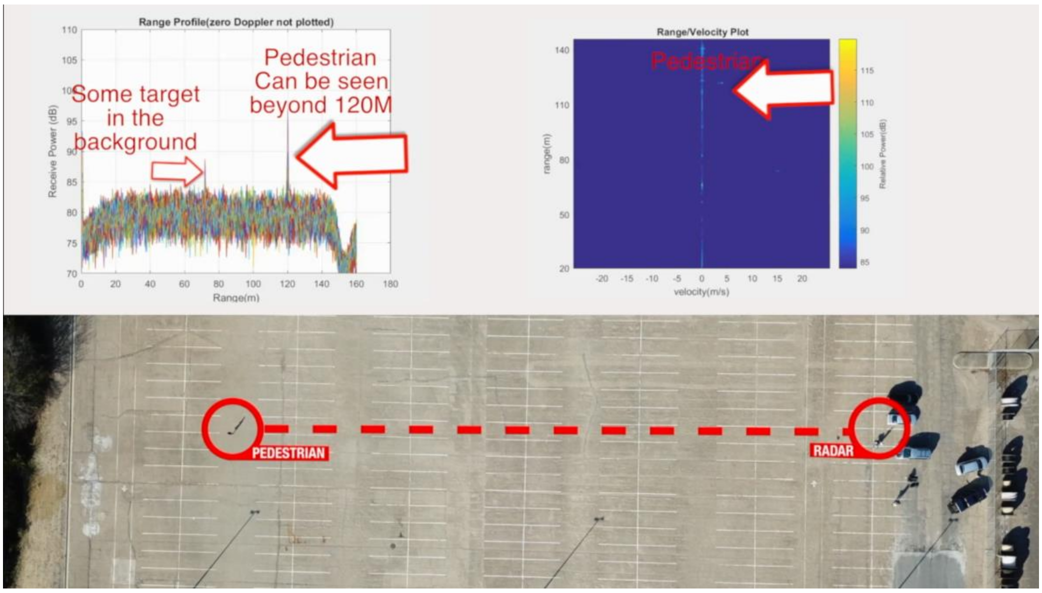

Fig 36: Detection of pedestrian beyond 120 meters

- **Detection of car beyond 250 meters**

In this test, the maximum detection range of a car is demonstrated by running 9TX beamforming. Results are shown in Fig 37. The car drives from one end of the parking lot to the other end, with total length around 270 meters. A drone is following the car to take the image during the entire course. The following picture shows that the car is still detected at 260 meters with SNR of 22 dB. Due to the space limitation, the test cannot continue beyond 270 meters.

Fig 37: Detection of car beyond 250 meters

- **Detection of car beyond 350 meters**

In this test, the maximum detection range of a car is demonstrated by running 9TX beamforming with a much longer test field. Results are shown in Fig 38. The car drives from 150 meters till the end of test track, with total length around 500 meters. The picture is taken when the car is too far to be caught by the camera lens. The following picture shows that the car is still detected at 370 meters with SNR of 14 dB.

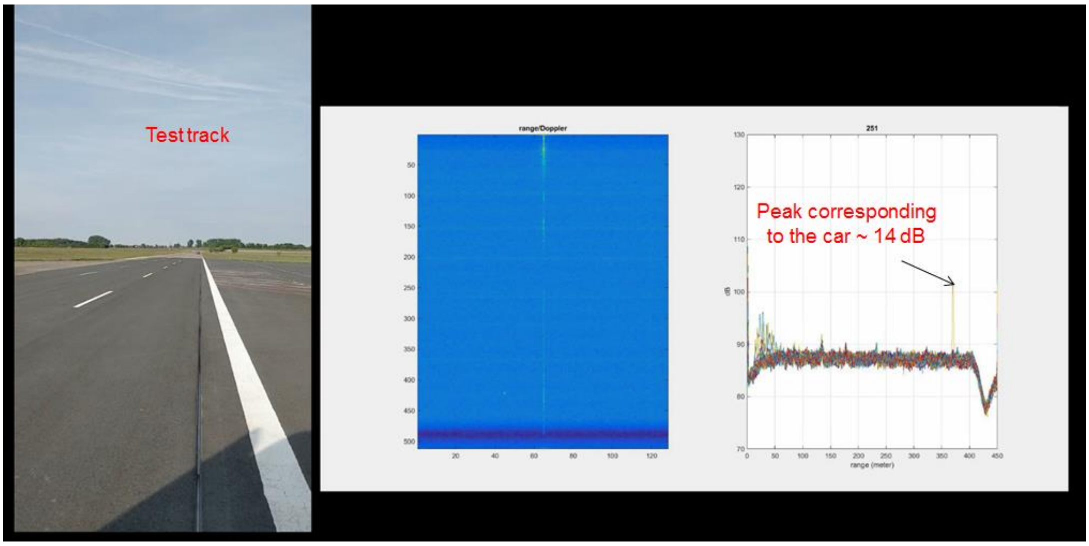

Fig 38: Detection of car beyond 350 meters

References:

[1] “Minimum-redundancy linear arrays”, A. Moffet, IEEE Transactions on Antennas and Propagation (Vol.16 (2), 1968)